$$\Delta f_{off} = \frac{\overline{\Delta\phi}(w_1)}{2\pi w_1 T_s} \tag{14}$$

and

$$\Delta f_{LW} = \frac{\sigma^2_{\Delta\phi,k}(w_2) - \sigma^2_{\Delta\phi,k}(w_1)}{4\pi(w_2 - w_1)T_s} \tag{15}$$

The statistics of the phase difference $\Delta\phi(w_1)$ also allow us to simultaneously and independently monitor the number of spans *N*, fiber nonlinear parameters as well as OSNR of the link. In particular, if we choose $w_1 = \eta$, the two samples $\phi(t)$ and $\phi(t + w_1 T_s)$ will belong to different pilot symbols with different power levels. In this case, the mean of the phase difference will be given by

$$\overline{\Delta\phi(\eta)} = (P_2 - P_1)N(\Lambda_S + \Lambda_D) + 2\pi\Delta f_{off} T \tag{16}$$

assuming the signal power at time *t* is $P(t) = P_1$.

As the parameters of SMF such as length, attenuation and nonlinear coefficients are usually known and relatively more consistent across a network compared to those of DCF in practice, we will assume the knowledge of σ_S^2 and Λ_S when monitoring the number of span *N*, fiber nonlinear coefficient and OSNR of the link. With Eqs. (2), (5), (8), (12)-(16) and some algebraic manipulations, one obtain

$$\begin{aligned} 2(P_1+P_2)\sigma_S^2\left(\Lambda_S^2 - \Lambda_S\frac{\overline{\Delta\phi(\eta)}}{P_1-P_2}\right)N^3 + \Bigg[(P_1+P_2)\frac{\overline{\Delta\phi(\eta)}^2\sigma^2_{power}(P_1)}{3(P_1-P_2)^2P_1} + 2(P_1+P_2)\sigma_S^2\frac{\overline{\Delta\phi(\eta)}^2}{(P_1-P_2)^2} \\ -2(P_1+P_2)\Lambda_S\sigma_S^2\frac{\overline{\Delta\phi(\eta)}}{P_1-P} + \frac{\sigma^2_{power}(P_1)}{4P_1}\left(\frac{1}{P_1}+\frac{1}{P_2}\right) - \left(\sigma^2_{\Delta\phi,1}(w_1) + \sigma^2_{\Delta\phi,2}(w_2)\right)\Bigg]N^2 \\ -\frac{(P_1+P_2)\overline{\Delta\phi(\eta)}^2\sigma^2_{power}(P_1)}{2P_1(P_1-P_2)^2}N + \frac{(P_1+P_2)\overline{\Delta\phi(\eta)}^2\sigma^2_{power}(P_1)}{6P_1(P_1-P_2)^2} = 0 \end{aligned} \tag{17}$$

which is a cubic function of *N*. Subsequently, the fiber nonlinear parameter Λ_D and OSNR can be calculated by

$$\Lambda_D = \frac{\overline{\Delta\phi(\eta)} - 2\pi\Delta f_{off} T}{(P_1 - P_2)N} - \Lambda_S \tag{18}$$

and

$$\text{OSNR} = \frac{P_k}{N(\sigma_S^2 + \sigma_D^2)} = \frac{P_k}{\frac{\sigma^2_{power}}{2P_k}} = \frac{2P_k^2}{\sigma^2_{power}} \qquad \text{for } k = 1, 2. \tag{19}$$

In summary, we can estimate frequency offset, laser linewidth, number of spans, fiber nonlinear parameter and OSNR of a transmission llink by choosing arbitrary values of P_1, P_2, w_1 and w_2 and solving for Eqs. (14), (15), (17), (18) and (19).

#135675 - $15.00 USD Received 27 Sep 2010; revised 21 Oct 2010; accepted 21 Oct 2010; published 26 Oct 2010

3. Simulation Results and Discussions

Simulations are conducted to investigate the monitoring performance of Δf_{off} , Δf_{LW} ,N, Λ_D and OSNR. Pilot sequences with 10^6 symbols with NRZ pulse shape are transmitted at two arbitrarily chosen power levels of $P_1 = -3$ dBm and $P_2 = -2$ dBm. The symbol rate is chosen to be 50 MSym/s so that the effects of CD and PMD become negligible. The sampling rate is set to be 25 GHz and thus $\eta = 500$. In our simulations, high analog-to-digital converter resolution (ADC) and timing recovery are assumed and other channel parameters are listed in Table 1. To maximize the monitoring range of Δf_{off} for a given sampling rate, w_1 is chosen to be 1. In addition, we arbitrarily set $w_2 = 3$ for laser linewidth monitoring. Simulation results for frequency offset and laser linewidth monitoring for a 15-span system are shown in Figs. 4(a) and 4(b) for full CD compensated and 10% CD under-compensated links. The means and standard deviations of the estimates are obtained from 10 independent trials with independent ASE noise. From the figures, the proposed technique enables a wide monitoring range from −10 GHz to 10GHz, more than sufficient for worst cases of ± 5 GHz reported in practical systems [18]. The corresponding maximum estimation error is below 6 MHz. For laser linewidth monitoring, a wide dynamic range of 100 kHz to 10 MHz with corresponding maximum estimation error below 1% is achieved. Such monitoring performance is comparable to others reported in the literature [4] that only monitors laser linewidths. It is also noted that the monitoring performance does not depend on the dispersion map of the transmission link.

Table 1. Channel parameters used in simulations

Parameter	Value	Parameter	Value
α_S	0.25 dB/km	α_D	0.6 dB/km
L_S	80 km	L_D	16 km for full CD compensation 14.4 km for 10% CD under-compensation
D_S	17 ps/km·nm	D_D	−85 ps/km·nm
n_{sp}	2	ν	193.1 THz
γ_S	1.2 W^{-1}/km		

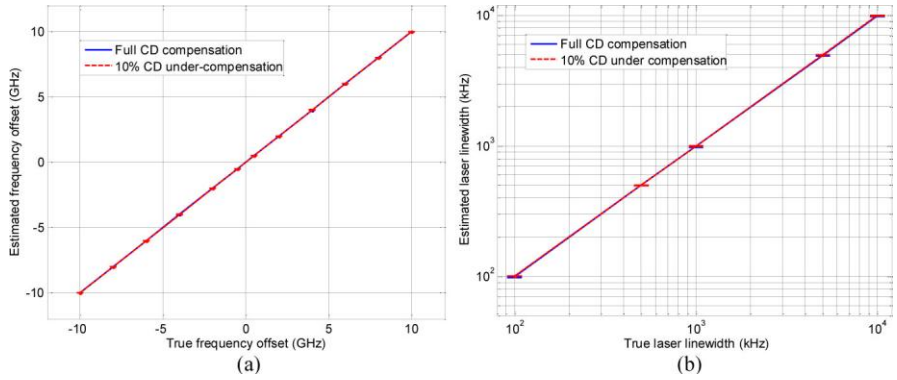

Fig. 4. (a) Estimated frequency offset vs. true frequency offset (b) Estimated laser linewidth vs. true laser linewidth for a 15-span system. Samples from 10^6 symbols are used for each estimate and the error bars indicate standard deviations of 10 independent estimates.

To ensure the monitoring accuracy of N, Λ_D and OSNR, the samples are further low-pass filtered with a bandwidth of 800 MHz and correspondingly down-sampled to eliminate the effect of CD on ASE noise. Figure 5 shows the estimated N, OSNR and Λ_D vs. their true

#135675 - $15.00 USD Received 27 Sep 2010; revised 21 Oct 2010; accepted 21 Oct 2010; published 26 Oct 2010

values for full CD compensated and 10% CD under-compensated links. The frequency offset and the laser linewidths are 200 MHz and 100 kHz respectively. As shown in Fig. 5(a), the mean of the estimated N generally agrees with their true values for $N \leq 22$. The slight inaccuracies for $N > 22$ may be caused by accumulated CD, frequency offset, laser linewidth, or a combination of them. Although the estimation errors gradually increase with N, the errors are limited to 1 span for a system containing around 25 spans. The OSNR monitoring accuracies shown in Fig. 5(b) for both dispersion maps with fiber nonlinearity are within 0.1 dB. The OSNR monitoring results are independent of the two dispersion maps and intra-channel nonlinearities. Figure 5(c) shows the estimated Λ_D for different values of Λ_D for a system with $N = 15$. Although estimation errors can be observed for both dispersion maps, the errors are limited to 0.4 dB and 0.6 dB (or equivalently 0.51 and 0.78 W^{-1}/km in γ_D) for full CD compensated and 10% CD under-compensated links respectively. In addition, it can also be shown that estimation remain fairly accurate when a few of spans have lengths slightly different than the rest of the link or when the knowledge of σ_S^2 and Λ_S is around 10% off from their true values.

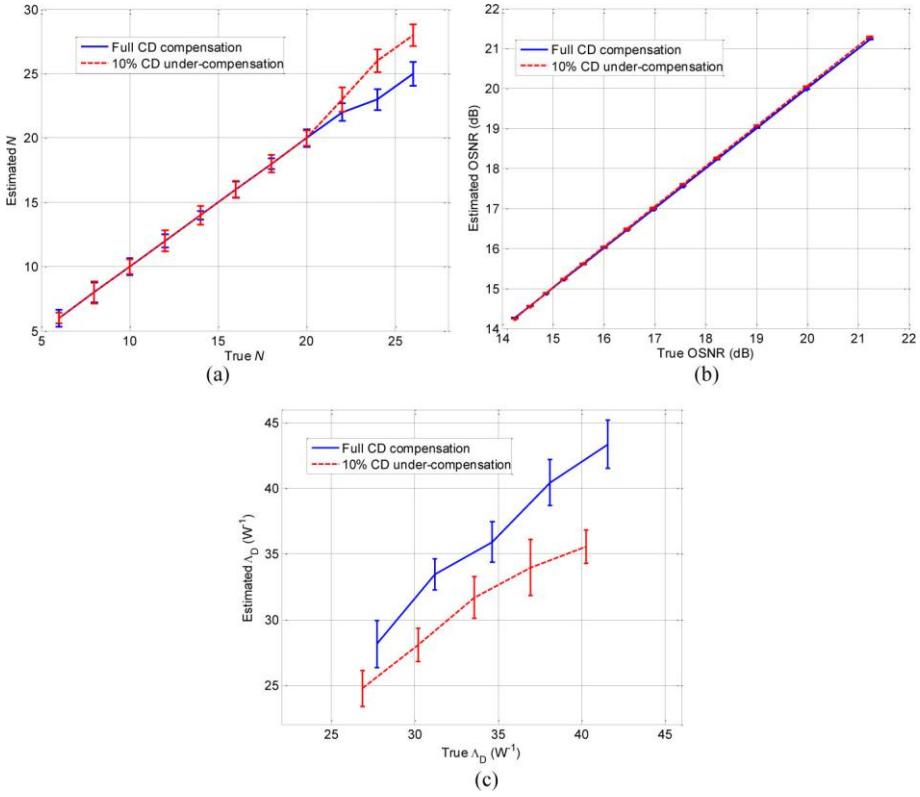

Fig. 5. (a) Estimated N vs. true N. (b) Estimated OSNR vs. true OSNR. (c) Estimated Λ_D vs. true Λ_D. Samples from 10^6 symbols are used for each estimate and the error bars indicate standard deviations of 10 independent estimates. The frequency offset and laser linewidth are 200 MHz and 100 kHz respectively.

4. Receiver-based fault localization using statistics of received pilot symbols

Data communications in optical networks can be interrupted by different types of faults along the link such as fiber cut, fiber bend and/or malfunctioning of inline optical amplifiers that result in sudden OSNR degradation or complete failure of the link. Locating the position of

#135675 - $15.00 USD Received 27 Sep 2010; revised 21 Oct 2010; accepted 21 Oct 2010; published 26 Oct 2010

such faults is crucial to network operators for efficient channel restoration and maintaining high quality of service (QoS) in dynamic network environments. When there is an undesired drop in signal power, the extra gain required to amplify the signal back to pre-determined levels will produce additional ASE noise which result in OSNR degradations at the receiver [19]. To locate faults, tunable optical time-domain reflectometer (OTDR) is proposed in [20] for the localization of fiber cut and serious degradation in OSNR. In [21], an optical transceiver is assigned to each predefined monitoring cycles to setup a dedicated supervisory channel. However, introduction of additional optoelectronic components will increase the cost of installation and maintenance, especially in large scale networks. Meanwhile, Sichani *et al.* [22] demonstrated the use of limited-perimeter vector matching fault-localization protocol to achieve efficient fault localization in large scale networks by analyzing the alarm message issued by multiple devices. One disadvantage of this approach is that at least two distinct lightpaths with separate source-destination pairs are required [23].

If we regularly insert the pilot symbols studied in this paper between data transmission, it is actually possible to locate faults without the need of monitoring equipments at intermediate points of the link by studying the changes in the statistics of the received signal power and phase difference. In particular from Eqs. (2) and (8), if sudden OSNR degradations occur at the i^{th} span, the increase in the ASE noise power of the i^{th} amplifier $\Delta\sigma_i^2$ will induce the same change in the received power variance $\Delta\sigma_{power}^2(P_k)$ regardless of the value of i. However, the induced change in the variance of phase difference $\Delta\sigma_{\Delta\phi,k}^2(1)$ will actually depend on i. Intuitively, this is because ASE noise introduced earlier in the transmission link undergoes more fiber nonlinear effects and accumulates more nonlinear phase noise. Therefore, by monitoring $\Delta\sigma_{power}^2(P_k)$ and $\Delta\sigma_{\Delta\phi,k}^2(1)$ due to sudden OSNR degradations, one can determine the amount and location of the additional ASE noise introduced in the link which in term serves as an indication of the location of the fault.

A calibration graph of the fault locations indexed according to the number of span starting from the transmitter vs. $\Delta\sigma_{\Delta\phi,k}^2(1)$ for different $\Delta\sigma_i^2$ is given in Fig. 6 for a 20-span link. The other parameters of the pilot sequence and the channel used in the simulation are identical to those in Section 3. From the figure, for a given $\Delta\sigma_i^2$, the change in variance of phase difference $\Delta\sigma_{\Delta\phi,k}^2(1)$ is distinct for different fault locations. In a network where fault locations are detected through other means, the proposed method may provide additional information about the status of the network and simplify network layer communication protocols and enhance efficiencies in network management.

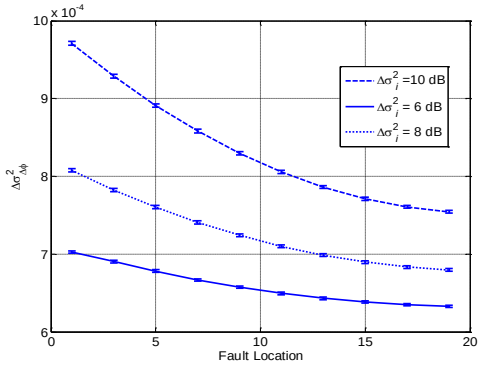

Fig. 6. Change in variance of phase difference $\Delta\sigma_{\Delta\phi}^2(1)$ vs. fault location with $\Delta\sigma_i^2 =$, 8 and 10 dB for a 20-span link. Samples from 10^6 symbols are used for each estimate and the error bars indicate standard deviations of 10 independent estimates.

#135675 - $15.00 USD Received 27 Sep 2010; revised 21 Oct 2010; accepted 21 Oct 2010; published 26 Oct 2010

5. Conclusions

In this paper, we demonstrated that DSP-based coherent communication systems require detail and accurate knowledge of transmission link parameters for appropriate and practical implementation of advanced impairment compensation algorithms such as digital back-propagation. We then proposed the use of pilot symbols prior to data transmission and study the statistics of the received power and phase difference to monitor laser frequency offset, laser linewidth, the number of spans, the fiber nonlinear parameters as well as the OSNR of the link. For links with full CD compensation or 10% CD under-compensation per span, simulation results indicated that simultaneous and independent monitoring of multiple parameters can be achieved with good monitoring range and accuracies. In addition, examining the changes in the statistics of received power and phase difference enable us to locate faults along a given transmission link without the need for monitoring equipments at intermediate nodes of the link. Experimental verifications of the proposed monitoring technique, impact of inhomogeneous fiber configuration, multi-parameter monitoring for CD-uncompensated links and the effect of WDM will be investigated in future.

Acknowledgments

The authors would like to acknowledge the support of the Hong Kong Government General Research Fund under project number 519910.

#135675 - $15.00 USD Received 27 Sep 2010; revised 21 Oct 2010; accepted 21 Oct 2010; published 26 Oct 2010